Electronic Supplementary Information (ESI)

Oxygen Vacancy-Engineered Fe_2O_3 Nanocubes *via* a Task-Specific Ionic Liquid for Electrocatalytic N_2 Fixation

Chenyun Zhang, Shuai Liu, Tingting Chen, Zhonghao Li,* Jingcheng Hao

Key Laboratory of Colloid and Interface Chemistry, Ministry of Education, Shandong University, Jinan, 250100, P. R. China, E-mail: zhonghaoli@sdu.edu.cn

Experimental Section

Chemical and materials

Hydrazine monohydrate ($N_2H_4 \cdot H_2O$, purity 98.0%), salicylic acid ($C_7H_6O_3$) as well as octylamine ($C_8H_{17}NH_2$) (molecular purity≥ 99%) were purchased from Aladdin Chemistry Co., Ltd. Formic acid (HCOOH, purity 98%), hydrated iron (III) chloride ($FeCl_3 \cdot 6H_2O$, purity ≥ 98%), potassium hydroxide (KOH, purity ≥ 96%), sodium sulfate (Na_2SO_4, purity ≥ 96%), sodium hydroxide (NaOH, purity ≥ 96%), ammonium chloride (NH_4Cl, purity ≥ 96%), hydrochloric acid (HCl, 36~38%), ethanol (C_2H_5OH, purity ≥ 99.7%), sulfuric acid (H_2SO_4, 96~98%), *p*-dimethylaminobenzaldehyde ($C_9H_{11}NO$, purity ≥ 98.0%), trisodium citrate dehydrate ($C_6H_5Na_3O_7 \cdot 2H_2O$, purity ≥ 99%) were obtained from Sinopharm Chemical Reagent Co., Ltd. Carbon cloth was gotten from Changsha Lyrun Material Co., Ltd. Nafion solution, Nafion 211 film and sodium nitroferricyanide dehydrate ($C_5FeN_6Na_2O \cdot 2H_2O$, purity ≥ 99%) were purchased from Sigma-Aldrich. Argon (Ar, purity 99.999%) and nitrogen (N_2, purity 99.999%) were obtained from Jinan Deyang Special gas Co., Ltd. $^{15}N_2$ gas (purity 99%) in cylinder was obtained from Wuhan Newradar Special Gas Co., Ltd. Sodium hypochlorite solution (NaClO, available chlorine 4.0%) was bought from Shanghai Macklin Biochemical Co., Ltd.

Preparation of ionic liquid (*n*-octylammonium formate, OAF)

25.85 g (0.2 mol) *n*-octylamine was added into a flask under vigorous stirring in an ice bath. Then, 9.20 g (0.2 mol) HCOOH was added dropwise to the flask until it became a white solid. The synthesized OAF was kept in a vacuum oven, mp 34 ^{o}C.

Synthesis of Fe_2O_3 in OAF or in water

In a typical procedure, 30 mg (1.1×10^{-4} mol) $FeCl_3 \cdot 6H_2O$ was added to 4 g (0.023 mol) OAF in teflon-lined stainless autoclave, which was held at 180 ^oC for 12 h. Then the autoclave was naturally cooled to ambient temperature after reaction. The obtained materials were washed using water as well as ethanol for four times, respectively. The synthesized product was then placed in a vacuum oven for 12 h at room temperature. Solid red power was donated as Fe_2O_3-IL. For comparison, synthesis of Fe_2O_3 in water was carried out using the similar method (denoted as Fe_2O_3-H_2O).

Material Characterization

Transmission electron microscopy (TEM) characterization was tested on a JEM 1400 TEM. X-ray diffraction (XRD) characterization was collected on Bruker D8A A25 X-ray Diffractometer. Energy-dispersive X-ray analysis (EDX) as well as EDX mapping were performed on OXFORD-instruments X-MaxN. X-ray photoelectron spectroscopy (XPS) measurements were conducted with a photoelectron spectrometer ESCALAB 250 XI. The photoluminescence spectroscopy (PLS) was measured by FLS 980 fluorescence spectrometer. UV-Vis spectra were operated using a SHIMADZU UV-2600 UV-Vis spectrophotometer. Fourier transformed infrared (FTIR) spectra were performed with Thermo Nicolet iS50 FT-IR. ^1H NMR experiments were performed on an Ascend400 spectrometer (400 MHz).

Electrochemical measurements

CHI model 760E electrochemical workstation was applied to measure the

electrochemical performance. Carbon cloth modified with Fe_2O_3 catalyst acted as working electrode, while Ag/AgCl electrode was employed as the reference electrode and graphite rod was used as the counter electrode. N_2 was prepurified by passing successively through acid solution (1 mM H_2SO_4) trap, distilled water trap and a molecular sieves column to remove any NO_x and NH_3 contamination before use.[1] N_2 electrochemical reduction was carried out in 0.1 M KOH or 0.1 M Na_2SO_4 solution with saturated nitrogen with respect to the reversible hydrogen electrode (RHE) at room temperature under atmospheric pressure. An absorber containing 0.001 M H_2SO_4 was connected to the alkaline electrolytic cell to avoid the overflow of ammonia from alkaline electrolyte, and the ammonia yield was the sum in the electrolyte and absorber. N_2 was purged into the KOH or Na_2SO_4 solution for at least 30 min to remove residual air. The chronoamperometric test was performed at applied potentials for 2 h. The electrochemical impedance spectroscopy (EIS) measurements were carried out with 5 mV of alternating voltage. The double-layer capacitance (C_{dl}) of iron oxide catalysts were offered by cyclic voltammetry (CV), measuring the double-layer capacitance from 0.1 to 0.2 V (*vs*. RHE) with the scanning rates ranging from 10 to 100 mV s^{-1}.

Working electrode was prepared as follows. Firstly, 5.0 mg Fe_2O_3 and 40 μL 5% Nafion solution were dispersed in 1000 μL deionized water with ultrasonicating for 0.5 h. Secondly, the 100 μL catalyst dispersion was coated on the 1 cm^{-2} carbon cloth (the mass loading of 0.5 mg cm^{-2}).

Determination of NH_3

The detection of NH_3 was made by ultraviolet spectrophotometry using salicylic acid.[2] 2 mL electrolyte or absorbing solution was obtained from the cathodic chamber or absorber. Then, the solution was mixed with 2 mL of 1 mol L^{-1} NaOH with sodium citrate (5 wt%) as well as salicylic acid (5 wt%). Finally, 1 mL of 0.05 mol L^{-1} NaClO as well as 0.2 mL $C_5FeN_6Na_2O$ (1 wt%) were added to the above solution. Absorbance measurements were carried out at λ = 655 nm. The concentration-absorbance curve was measured by applying the standard NH_4Cl solution with NH_4^+ concentrations with 0.0, 0.2, 0.4, 1.0, 2.0, 4.0, 6.0 μg mL^{-1}. The fitting curve offered a linear relation of absorbance value under different NH_3 concentration. The NH_3 concentration was obtained from the calibration curve.

Determination of N_2H_4

N_2H_4 production was obtained using the Watt and Chrisp method.[2] Mixing of para-(dimethylamino) benzaldehyde (0.599 g), HCl (12 mol L^{-1}, 3 mL) and ethanol (30 mL) obtained a color reagent. Concentration of N_2H_4 was determined as follows. 2 mL of the electrolyte after electrolysis was mixed with 2 mL of color reagent. The absorbance of solution occurred at 455 nm. The concentration-absorbance curve was adjusted with a series of hydrazine hydrate solution (0.0, 0.2, 0.5, 1.0, 2.0, 2.5 μg mL^{-1}). The fitting curve displayed a linear relationship of absorbance with the N_2H_4 concentration.

Determination of NH_3 formation rate

$$V_{NH_3} = [NH_3] \times V / t / m_{cat}$$

Where

$[NH_3]$: the obtained NH_3 concentration,

V: the volume of electrolyte or absorber collecting NH_3,

t: the time of reduction,

m_{cat}: catalyst mass.

Determination of Faradaic efficiency (FE)

Supposing three electrons were required to form an NH_3 molecule, FE could be gotten as follows:

$$FE = C_{NH_3} \times V \times N \times F / Q$$

Where

Q: quantity of electric charge connected by chronoamperometric test,

N: the number of electron transferred to form product (for NH_3 of 3),

F: Faraday constant, 96485 C mol^{-1},

C_{NH_3}: NH_3 concentration measured,

V: the volume of electrolyte.

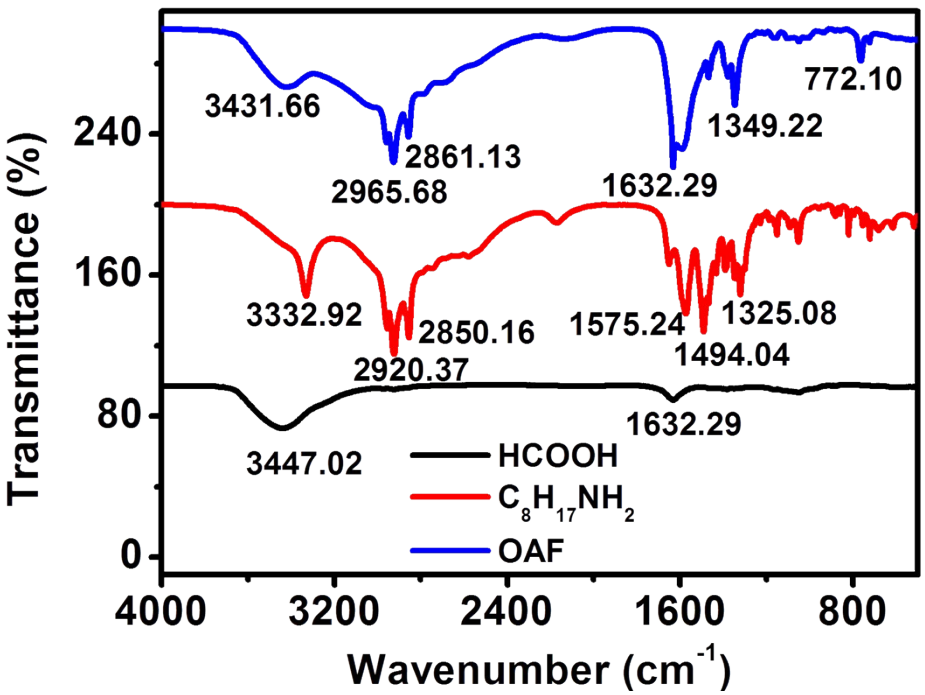

Fig. S1. FTIR spectra of the as-prepared ionic liquid *n*-octylammonium formate.

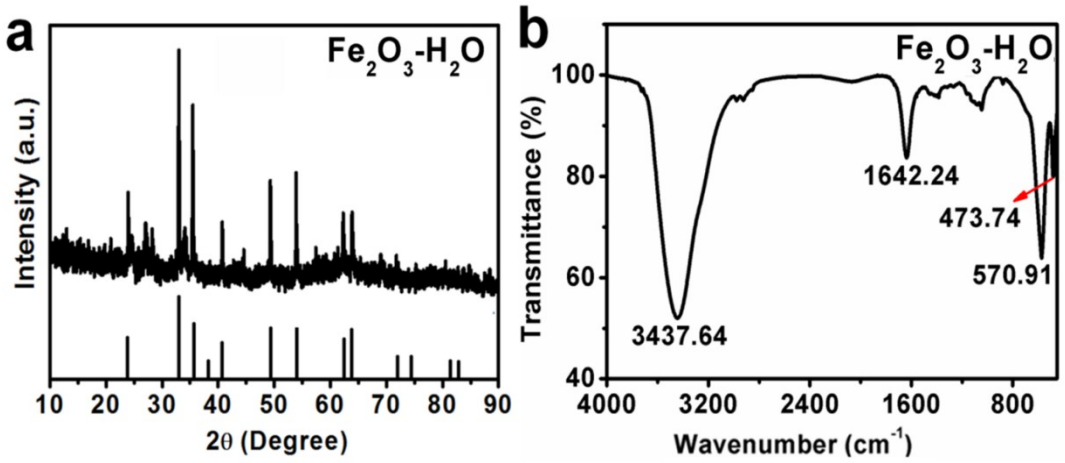

Fig. S2. XRD pattern (a) and FTIR spectrum (b) of Fe_2O_3-H_2O.

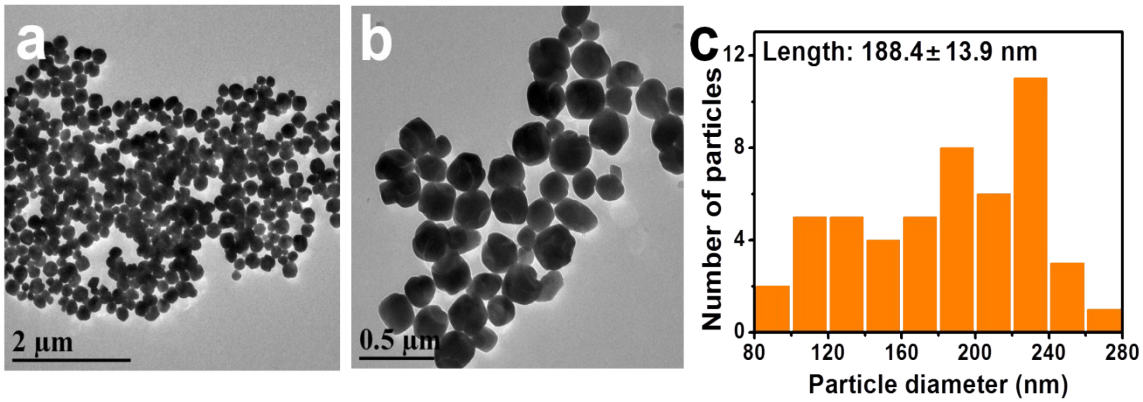

Fig. S3. The low- (a), high-magnification (b) TEM images and the particle size distribution (c) of Fe_2O_3-H_2O.

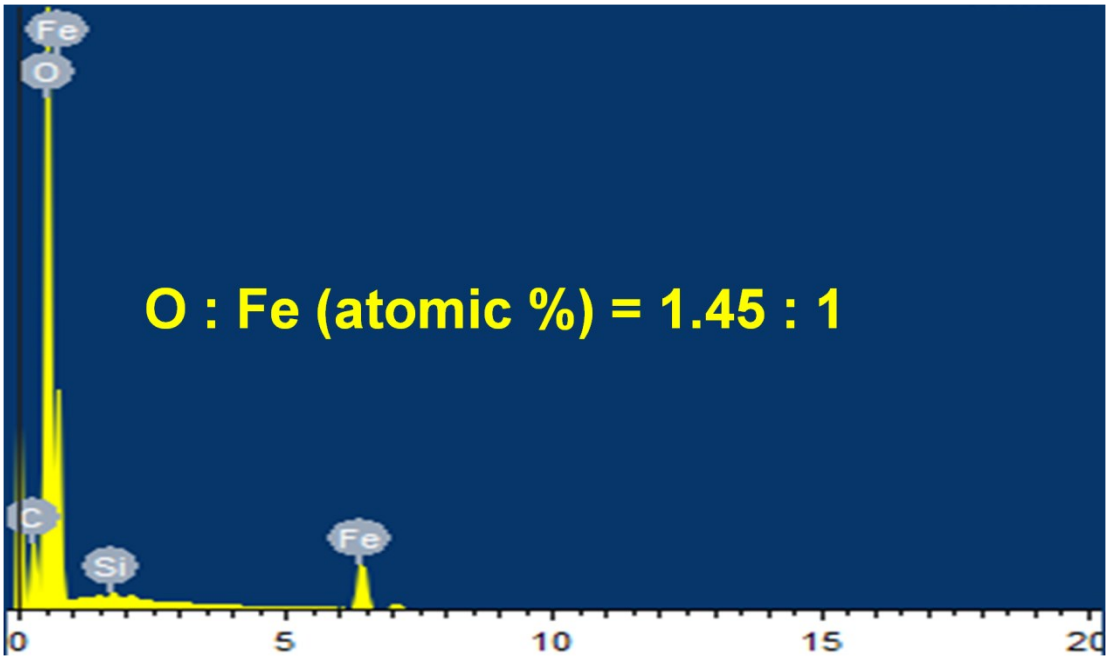

Fig. S4. EDX image of as-prepared Fe_2O_3-IL (O : Fe = 53.62 : 36.90).

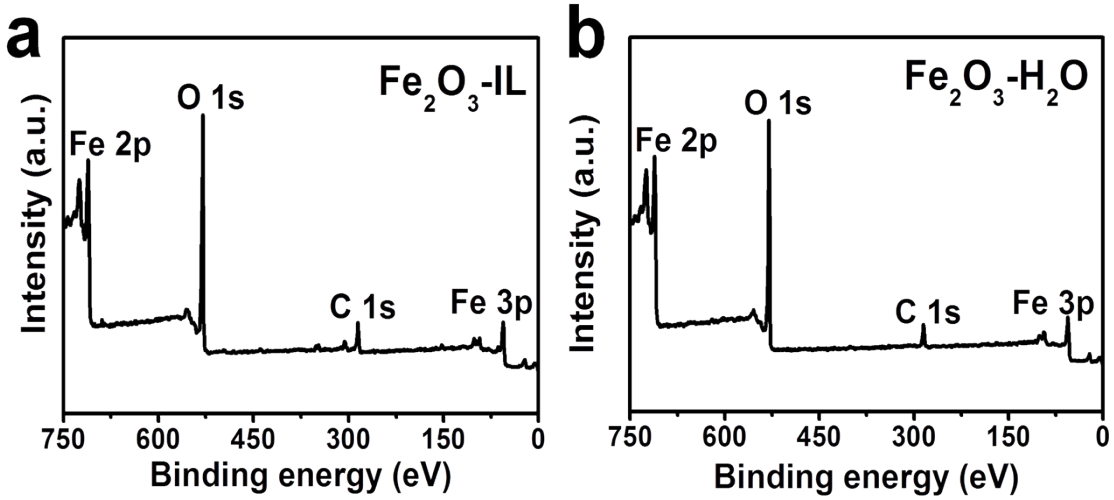

Fig. S5. XPS survey spectra of Fe_2O_3-IL (a) and Fe_2O_3-H_2O (b).

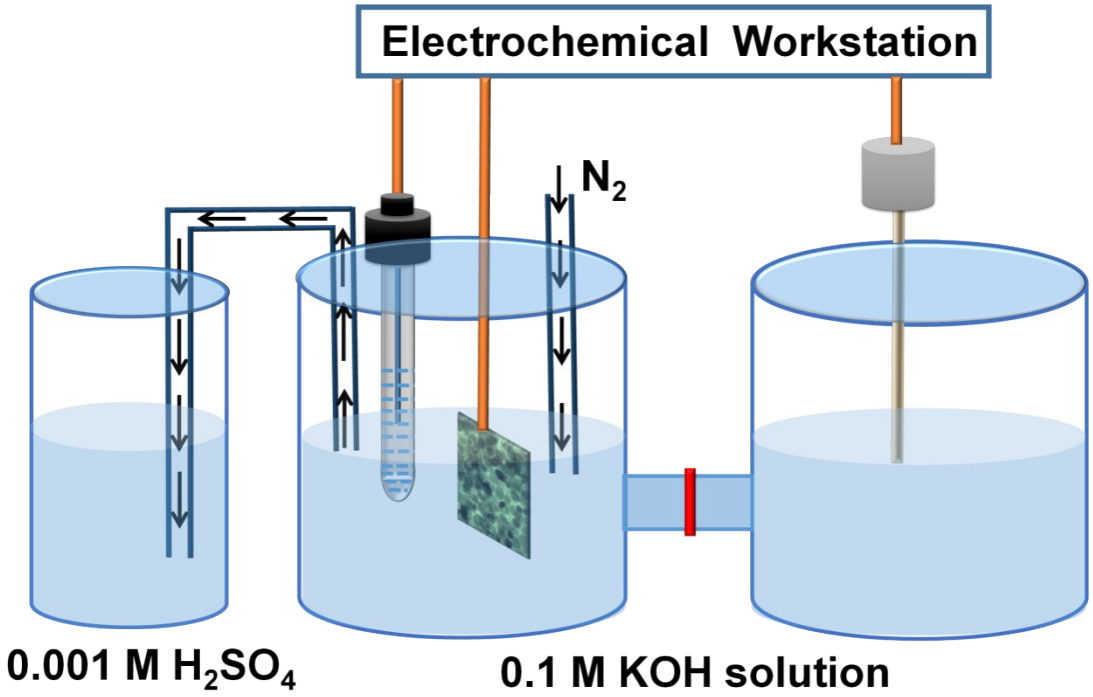

Fig. S6. The electrolytic device of alkaline electrolyte (0.1 M KOH solution).

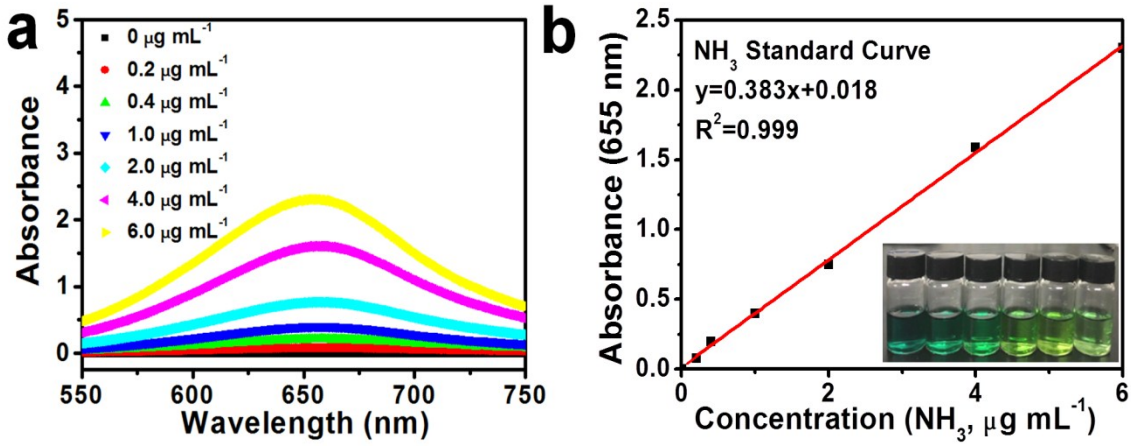

Fig. S7. In 0.1 M KOH electrolyte, the concentration-absorbance curve of NH_4^+ with concentration of 0.0, 0.2, 0.4, 1.0, 2.0, 4.0 and 6.0 μg mL^{-1} (a); calibration curve used for calculation of NH_3 by NH_4^+ concentration (b).

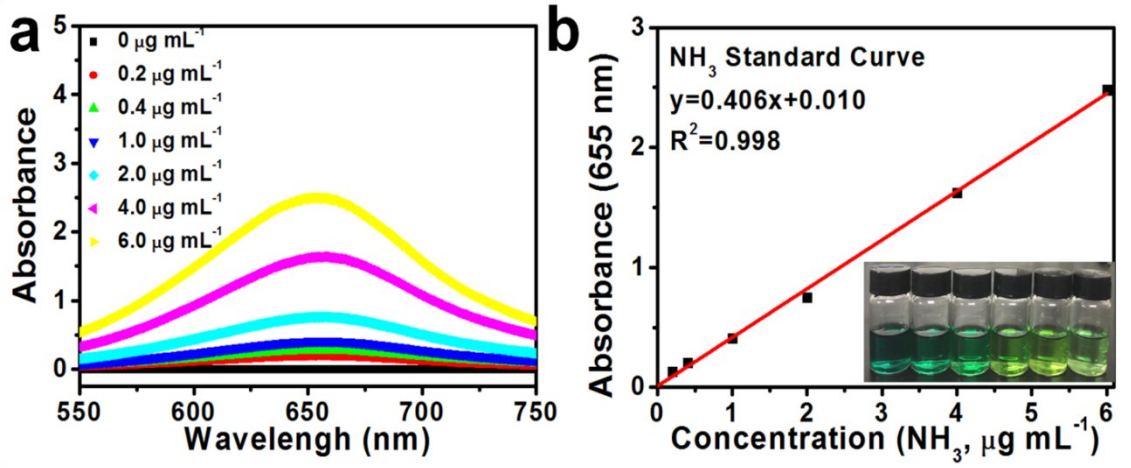

Fig. S8. In 0.001 M H_2SO_4 absorber, the concentration-absorbance curve of NH_4^+ with concentration of 0.0, 0.2, 0.4, 1.0, 2.0, 4.0 and 6.0 μg mL^{-1} (a); calibration curve used for calculation of NH_3 by NH_4^+ concentration (b).

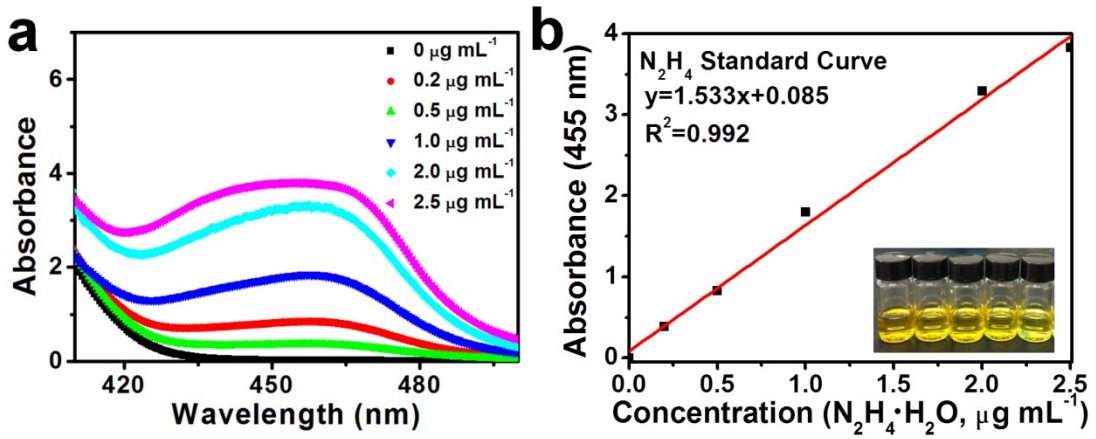

Fig. S9. In 0.1 M KOH electrolyte, the concentration-absorbance curve of N_2H_4 with concentration of 0.0, 0.2, 0.5, 1.0, 2.0 and 2.5 μg mL^{-1} (a); calibration curve used for calculation of N_2H_4 concentration (b).

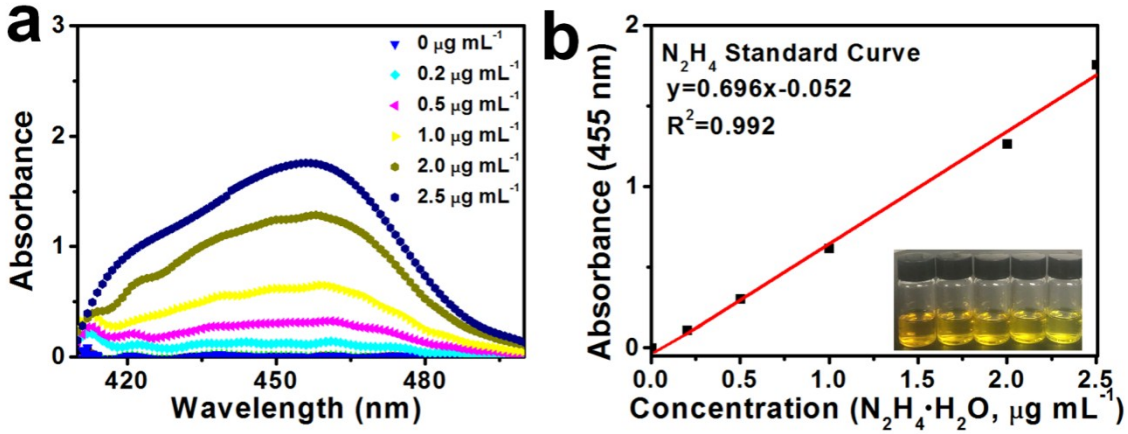

Fig. S10. In 0.001 M H_2SO_4 absorber, the concentration-absorbance curve of N_2H_4 with concentration of 0.0, 0.2, 0.5, 1.0, 2.0 and 2.5 μg mL^{-1} (a); calibration curve used for calculation of N_2H_4 concentration (b).

Table S1. NH_3 formation rates and the corresponding Faradaic efficiencies (FEs) of Fe_2O_3-IL under various potentials in 0.1 M KOH electrolyte.

Potential (V)	NH_3 formation rate ($\mu g\ h^{-1}\ mg^{-1}_{cat}$)	NH_3 formation rate ($mol\ s^{-1}\ cm^{-2}$)	FE (%)
0.0	8.55	6.99×10^{-11}	25.93
-0.1	22.01	1.80×10^{-10}	20.34
-0.2	19.40	1.59×10^{-10}	17.88
-0.3	32.13	2.62×10^{-10}	6.63
-0.4	30.61	2.50×10^{-10}	0.63
-0.5	35.55	2.91×10^{-10}	0.27

Table S2. Comparison of NRR performance for the different catalysts at room temperature and ambient pressure.

Catalyst	Electrolyte	Potential (V vs. RHE)	NH_3 formation rate	FE (%)	Ref.
γ -Fe_2O_3	0.1 M KOH	0.0	0.212 $\mu g\ h^{-1}\ mg^{-1}_{cat}$	1.9	3
Fe_2O_3	0.1 M Na_2SO_4	-0.8	15.9 $\mu g\ h^{-1}\ mg^{-1}_{cat}$	0.94	4
Fe_3O_4/Ti	0.1 M Na_2SO_4	-0.4	5.6×10^{-11} mol s^{-1} cm^{-2}	2.6	5
Fe/Fe_3O_4	0.1 M KOH	-0.3	3.10×10^{-12} mol s^{-1} cm^{-2}	8.29	6
Au	0.1 M KOH	-0.2	1.648 $\mu g\ h^{-1}\ cm^{-2}$	3.88	7
Rh	0.1 M KOH	-0.2	23.88 $\mu g\ h^{-1}\ mg^{-1}_{cat}$	0.217	8
MoS_2/CC	0.1 M Na_2SO_4	-0.5	8.08×10^{-11} mol s^{-1} cm^{-2}	1.17	9
$Ti_3C_2T_x$	0.5 M Li_2SO_4	-0.2	0.26 $\mu g\ h^{-1}\ mg^{-1}_{cat}$	5.78	10
TiO_2/Ti	0.1 M Na_2SO_4	-0.7	9.16×10^{-11} mol s^{-1} cm^{-2}	2.5	11
VN/Ti	0.1 M KOH	-0.5	8.40×10^{-11} mol s^{-1} cm^{-2}	2.25	12
NbO_2	0.05 M H_2SO_4	-0.6	4.07 $\mu g\ h^{-1}\ mg^{-1}_{cat}$	32	13

NbO_2	0.05 M H_2SO_4	-0.65	11.6 μg h^{-1} mg^{-1}_{cat}	19.7	13
Fe_2O_3-IL	**0.1 M KOH**	**-0.3**	**32.13 μg h^{-1} mg^{-1}_{cat} (2.62 × 10^{-10} mol s^{-1} cm^{-2})**	**6.63**	**Our work**

CNT = Carbon nanotube; CC = Carbon cloth

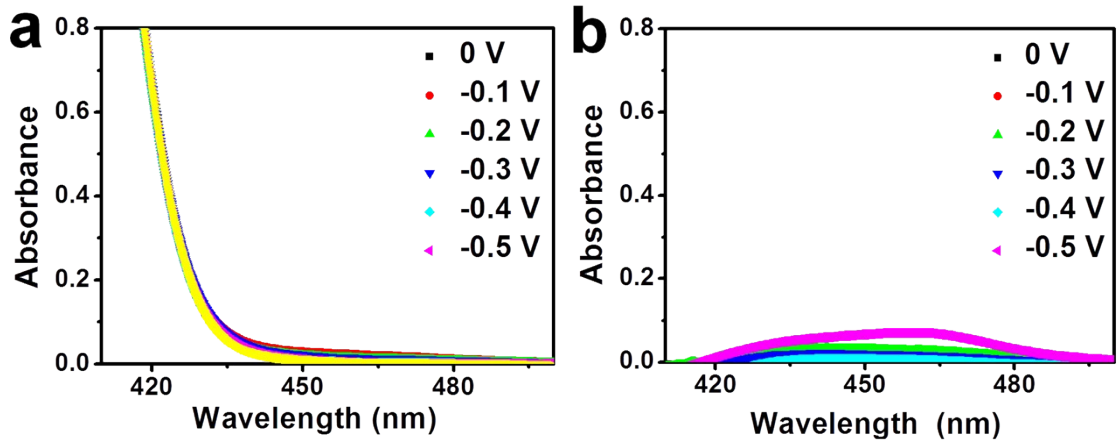

Fig. S11. The absorbance of hydrazine for Fe_2O_3-IL in 0.1 M KOH electrolyte (a) and 0.001 M H_2SO_4 absorber (b) under different potentials.

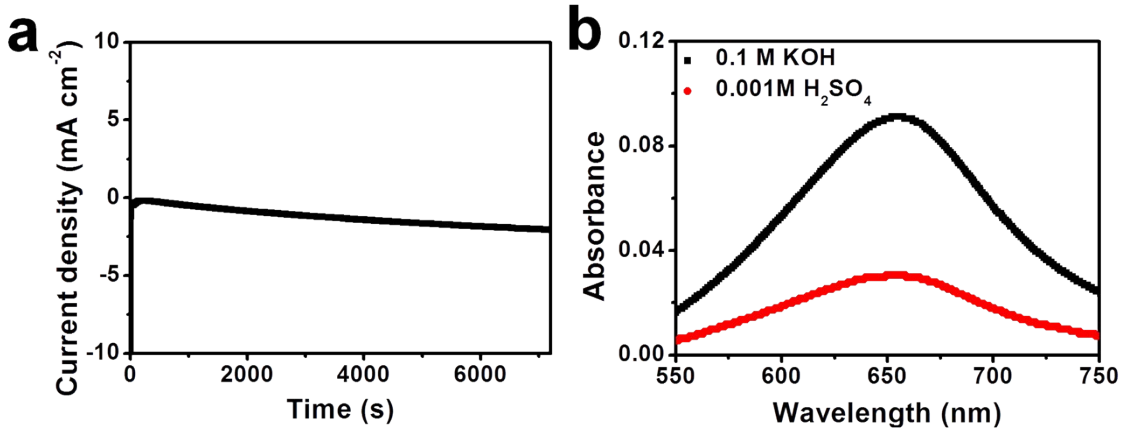

Fig. S12. The current density for Fe_2O_3-H_2O with the time range of 2 h at -0.30 V *vs.* RHE in alkaline electrolyte (a); the absorbance in 0.1 M KOH electrolyte and 0.001

M H_2SO_4 absorber (b).

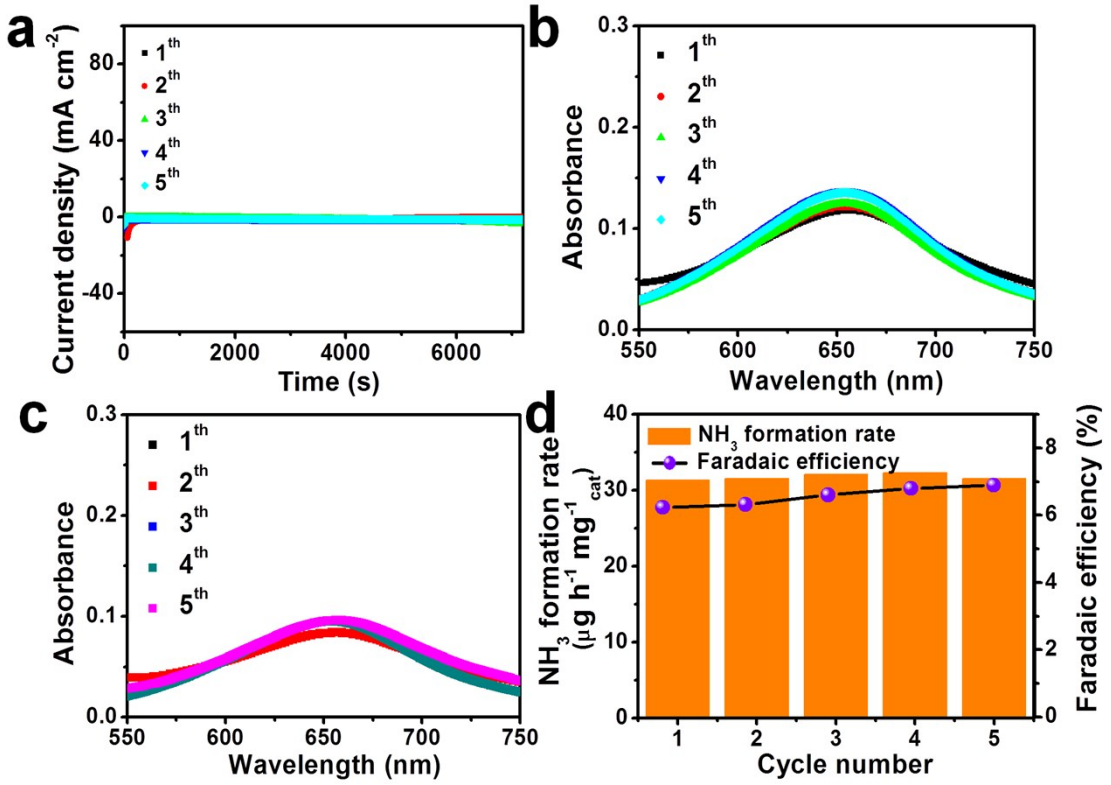

Fig. S13. The electrocatalytic stability of Fe_2O_3-IL at -0.30 V *vs.* RHE: the current densities under different cycles in alkaline electrolyte (a); absorbance under different cycles in 0.1 M KOH electrolyte (b); absorbance in 0.001 M H_2SO_4 absorber (c); NH_3 formation rates and FEs under different cycles (d).

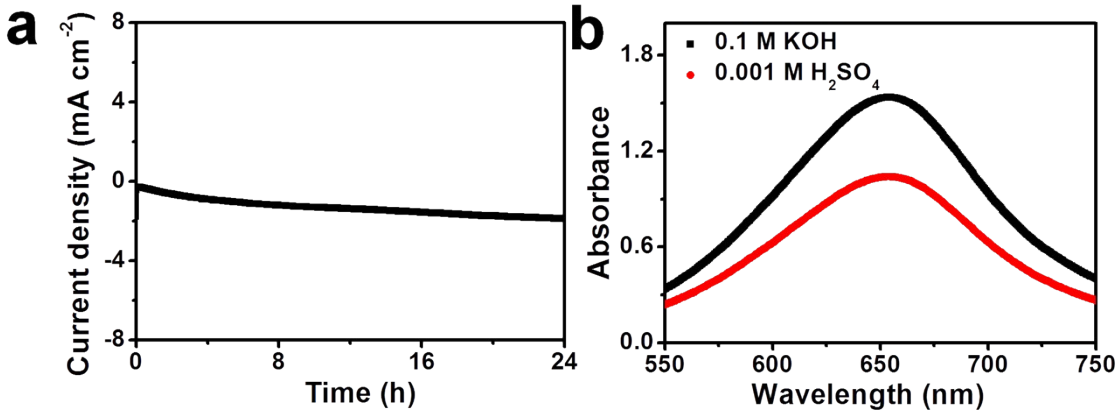

Fig. S14. Fe_2O_3-IL at -0.30 V *vs.* RHE: the corresponding of current density for 24 h

in alkaline electrolyte (a); the absorbance in 0.1 M KOH electrolyte and 0.001 M H_2SO_4 absorber (b).

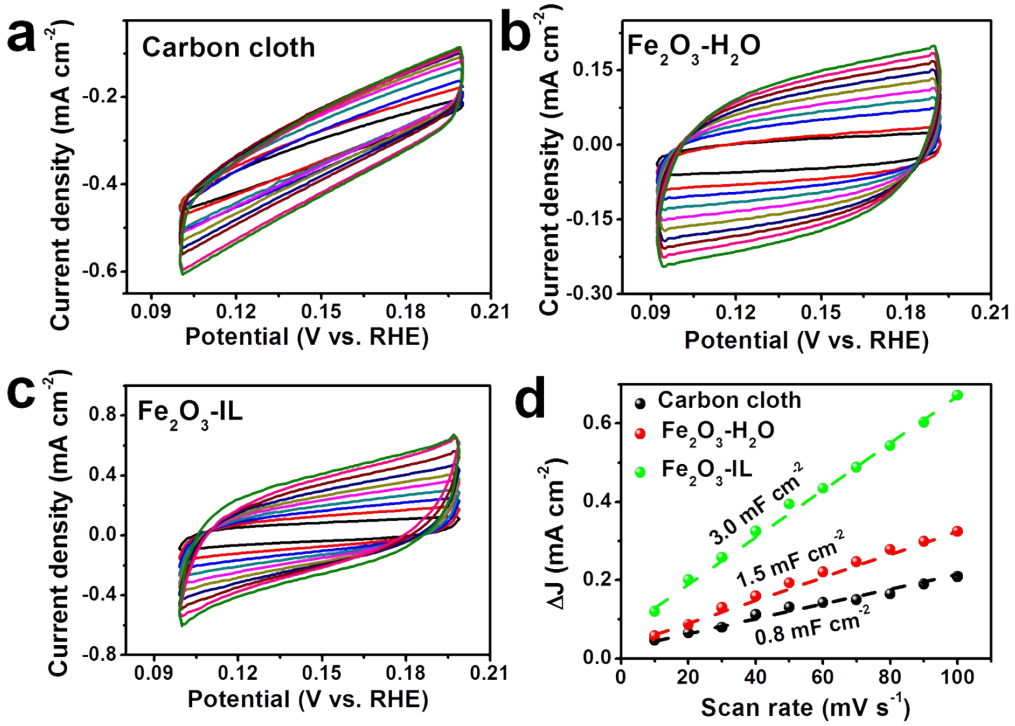

Fig. S15. Cyclic voltammograms at different scan rates of 10, 20, 30, 40, 50, 60, 70, 80, 90 and 100 mV s^{-1} in 0.1 M KOH electrolyte: carbon cloth (a), Fe_2O_3-H_2O (b), Fe_2O_3-IL (c); the double-layer capacitance (C_{dl}) (d).

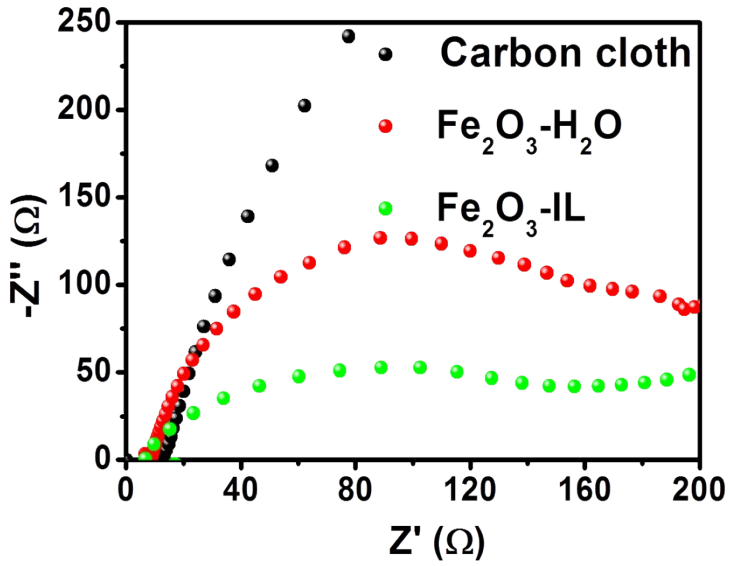

Fig. S16. Electrochemical impedance spectra (EIS) results of carbon cloth, Fe_2O_3-H_2O and Fe_2O_3-IL in 0.1 M KOH electrolyte.

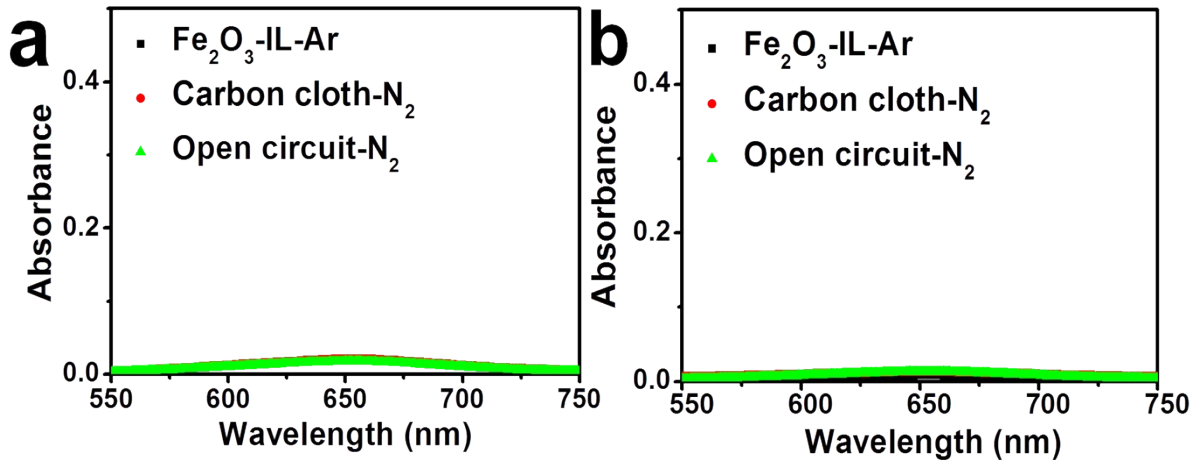

Fig. S17. Control experiments to verify the N source of the produced NH_3 at -0.30 V *vs.* RHE in 0.1 M KOH electrolyte (a) and in 0.001 M H_2SO_4 absorber (b). No apparent NH_3 was detected for the electrolysis with Ar-saturated electrolyte (Fe_2O_3-IL-Ar), without the Fe_2O_3-IL catalyst (Carbon cloth-N_2) and at the open circuit (Open circuit-N_2).

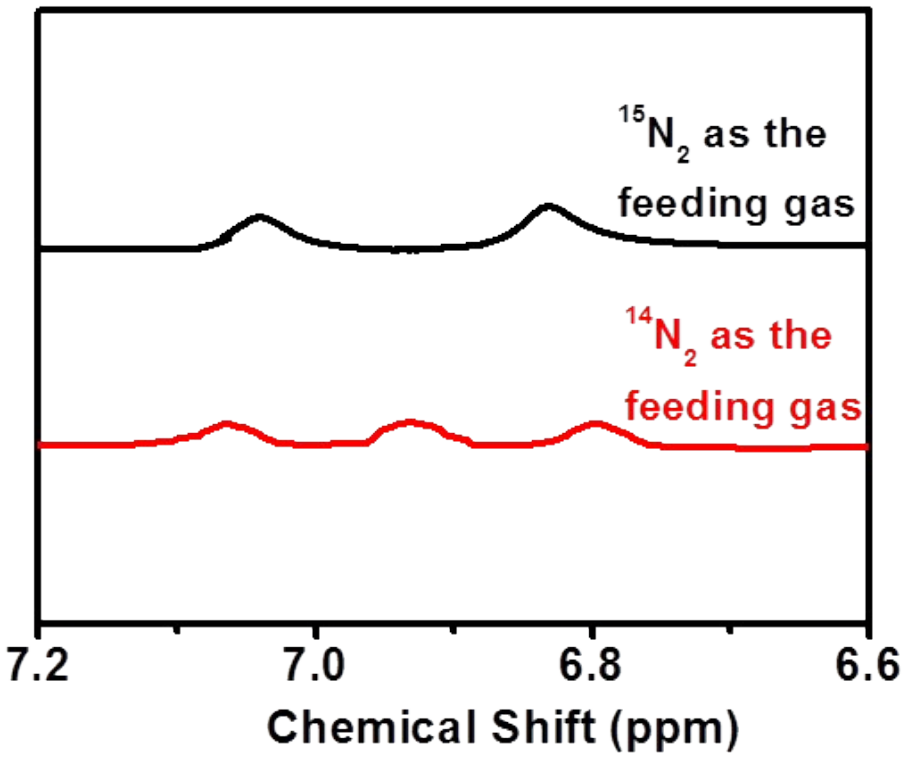

Fig. S18. ^{1}H NMR spectra for the $^{15}NH_4^+$ and $^{14}NH_4^+$ after electrolysis of Fe_2O_3-IL using $^{15}N_2$ and $^{14}N_2$ as the feeding gas, respectively.

As illustrated in Fig. S18, a triplet coupling for $^{14}NH_4^+$ and a doublet coupling for $^{15}NH_4^+$ were shown in the ^{1}H NMR spectra when used $^{14}N_2$ and $^{15}N_2$ as the feeding gas, respectively. ^{1}H NMR spectra revealed that $^{15}N_2$ as supplied gas only offered a doublet coupling of $^{15}NH_4^+$. It confirmed that NH_3 originated from the electrocatalytic N_2 reduction by Fe_2O_3-IL.

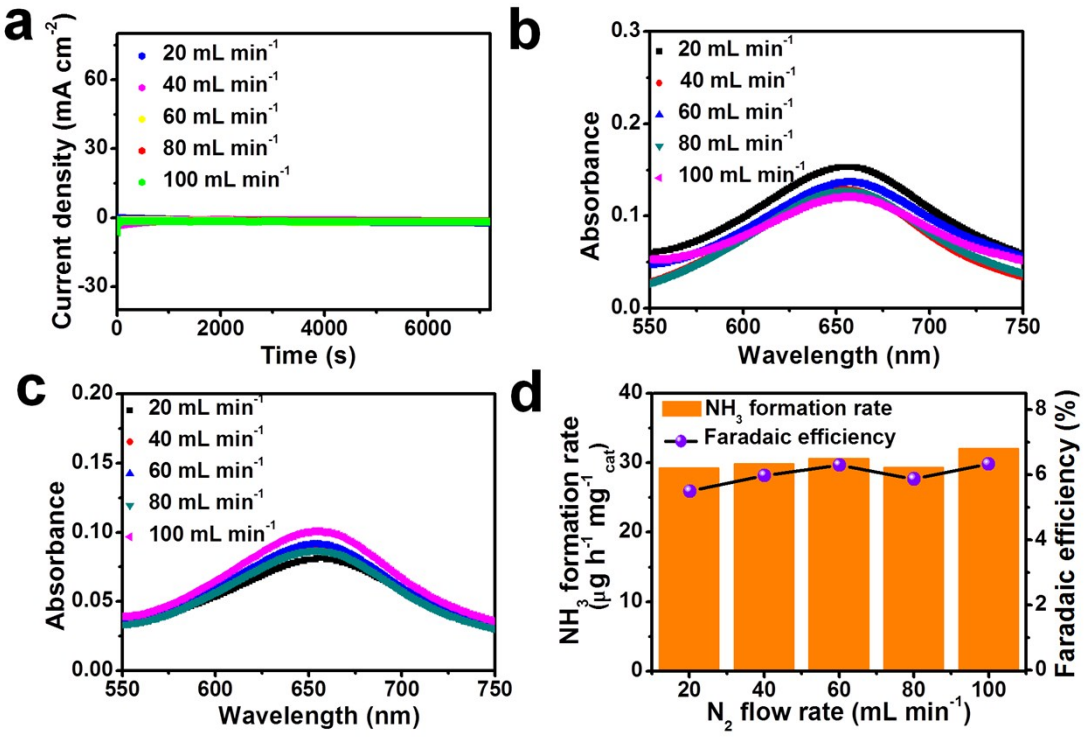

Fig. S19. Fe_2O_3-IL as catalyst at -0.30 V *vs.* RHE: the current densities under different nitrogen flow rates in 0.1 M KOH electrolyte (a); absorbance under different nitrogen flow rates in 0.1 M KOH electrolyte (b); absorbance in 0.001 M H_2SO_4 absorber (c); NH_3 formation rates and FEs under different nitrogen flow rates in 0.1 M KOH electrolyte (d).

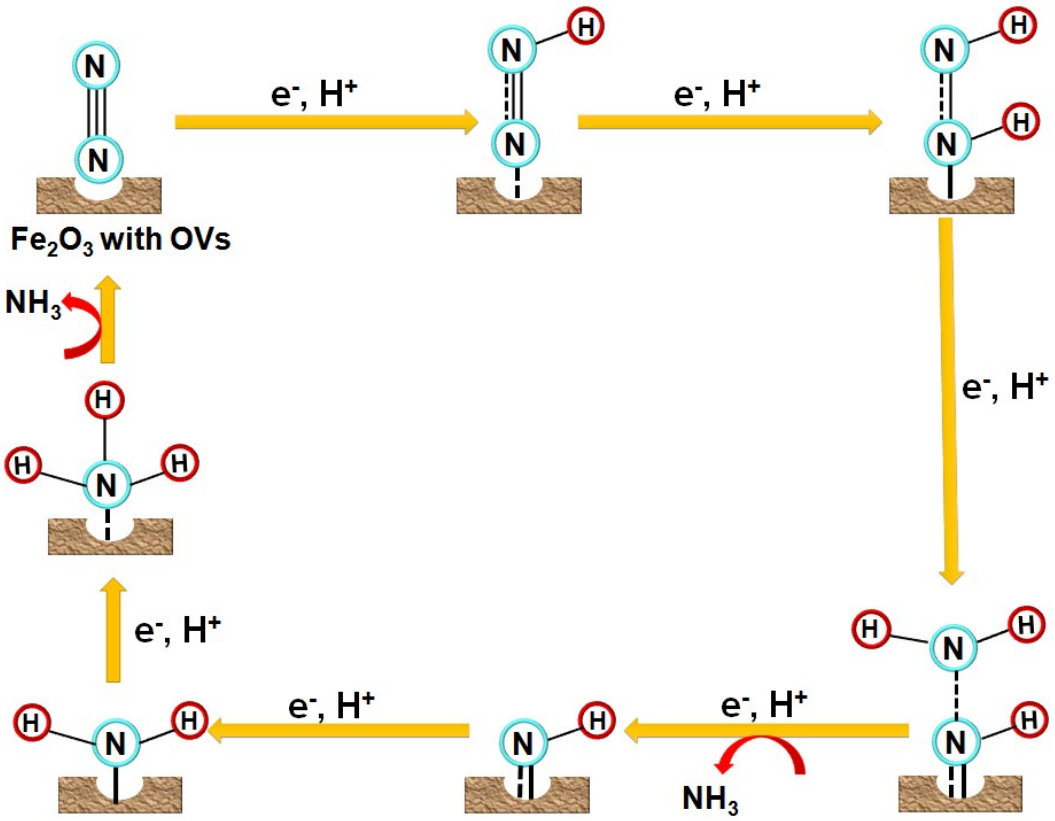

Fig. S20. Plausible mechanism of NRR catalyzed by hematite which has been proposed early by Nguyen *et al.*[14]

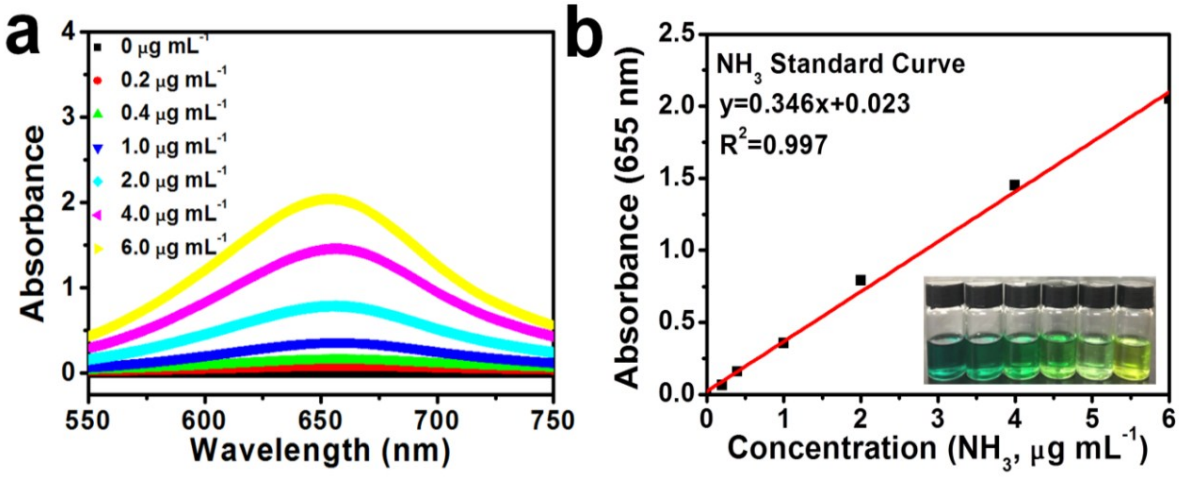

Fig. S21. In 0.1 M Na_2SO_4 electrolyte, the concentration-absorbance curve of NH_4^+ with concentration of 0.0, 0.2, 0.4, 1.0, 2.0, 4.0 and 6.0 μg mL^{-1} (a); calibration curve used for calculation of NH_3 by NH_4^+ concentration (b).

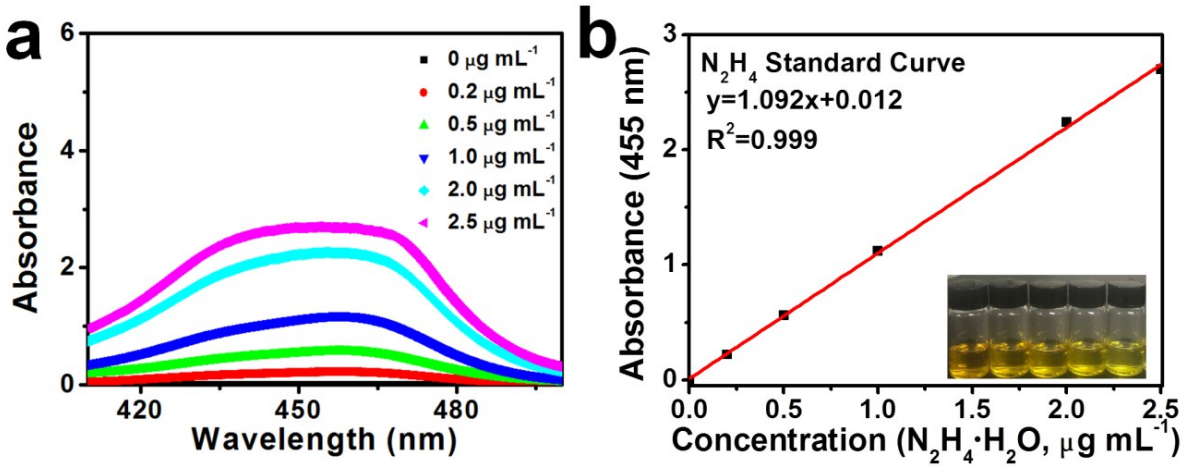

Fig. S22. In 0.1 M Na_2SO_4 electrolyte: the concentration-absorbance curve of N_2H_4 with concentration of 0.0, 0.2, 0.5, 1.0, 2.0 and 2.5 μg mL^{-1} (a); calibration curve used for calculation of N_2H_4 concentration (b).

Table S3. NH_3 formation rates and the corresponding FEs of Fe_2O_3-IL under various potentials in 0.1 M Na_2SO_4 electrolyte.

Potential (V)	NH_3 formation rate ($\mu g\ h^{-1}\ mg^{-1}_{cat}$)	NH_3 formation rate ($mol\ s^{-1}\ cm^{-2}$)	FE (%)
-0.4	3.21	2.63×10^{-11}	9.99
-0.5	2.99	2.45×10^{-11}	3.91
-0.6	3.32	2.71×10^{-11}	0.92
-0.7	12.30	1.00×10^{-10}	0.81
-0.8	24.81	2.02×10^{-10}	0.66
-0.9	25.77	2.11×10^{-10}	0.20

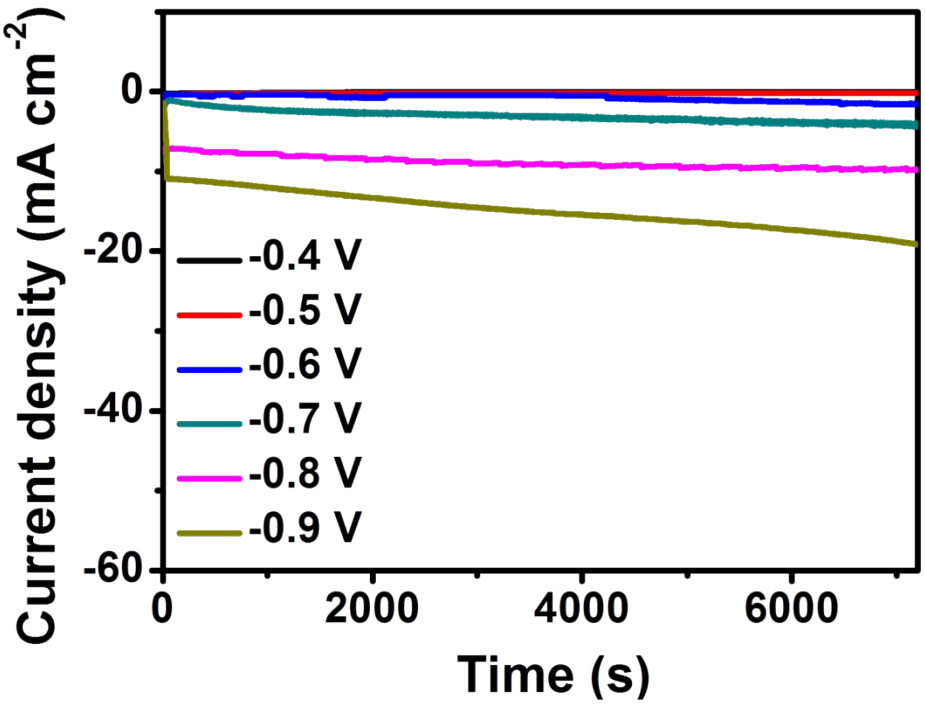

Fig. S23. The chronoamperometric test of Fe_2O_3-IL in 0.1 M Na_2SO_4 under the potentials from -0.4 V to -0.9 V for 2 h.

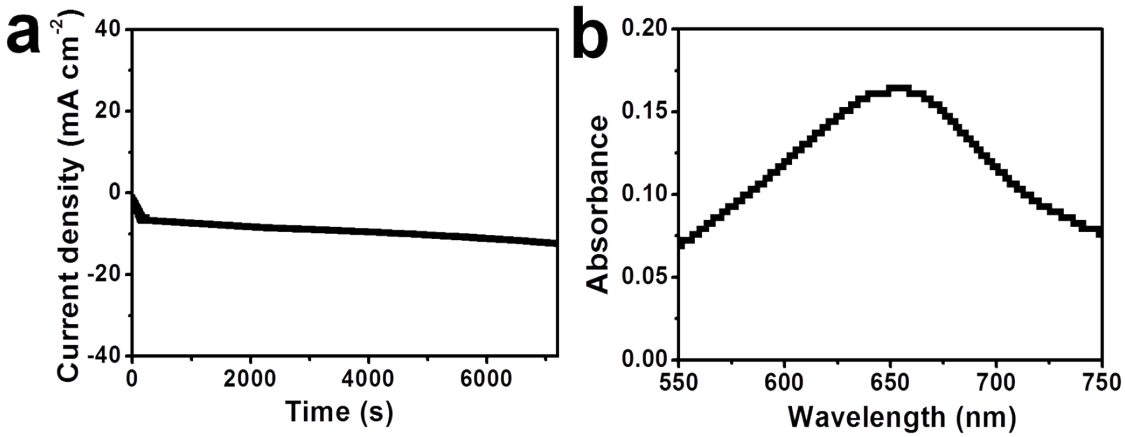

Fig. S24. Fe_2O_3-H_2O as catalyst in 0.1 M Na_2SO_4 electrolyte: the current densities at -0.8 V *vs.* RHE for 2 h (a); corresponding absorbance (b).

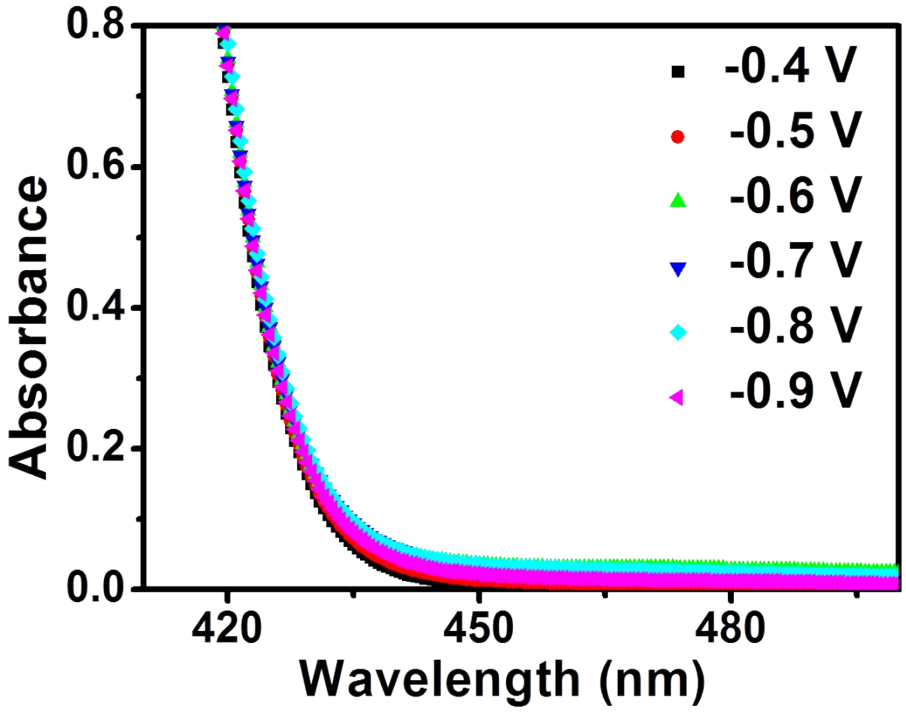

Fig. S25. The absorbance of hydrazine of Fe_2O_3-IL in 0.1 M Na_2SO_4 electrolyte under different potentials.

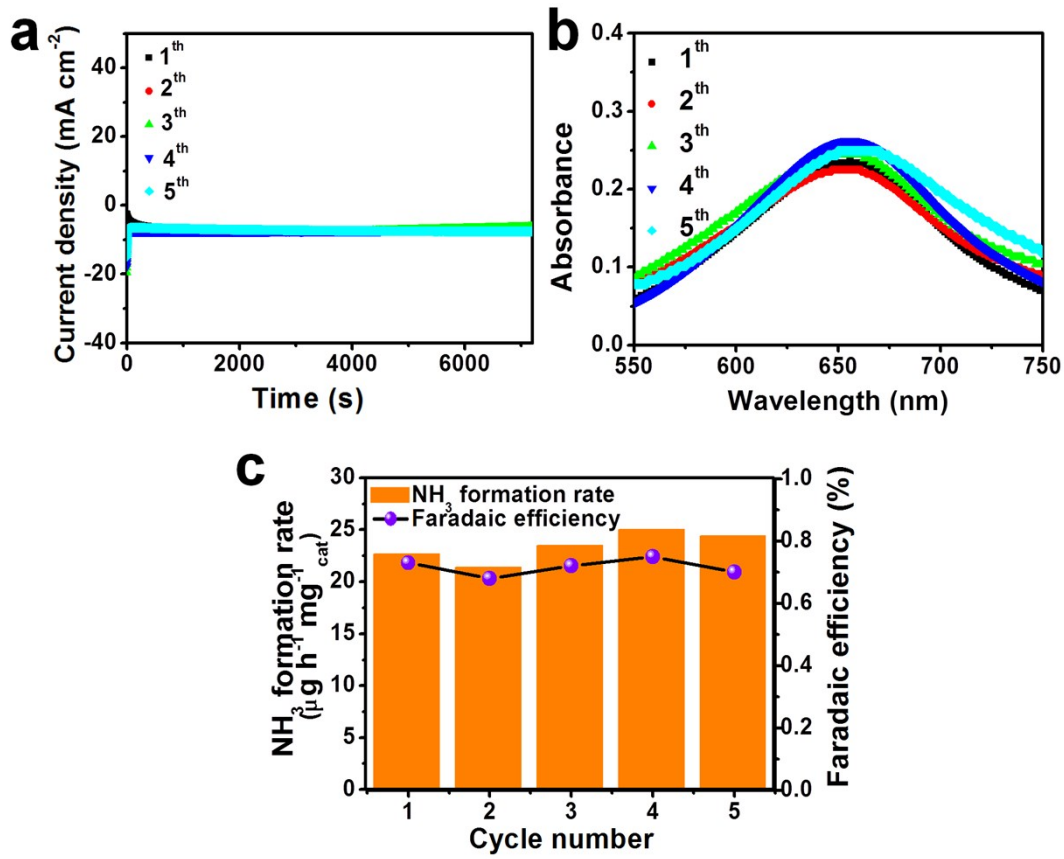

Fig. S26. Fe_2O_3-IL as catalyst: the electrocatalytic stability at -0.8 V *vs.* RHE in 0.1 M Na_2SO_4 electrolyte under different cycles, the current densities (a); the UV-Vis absorbance (b); NH_3 formation rates and FEs (c).

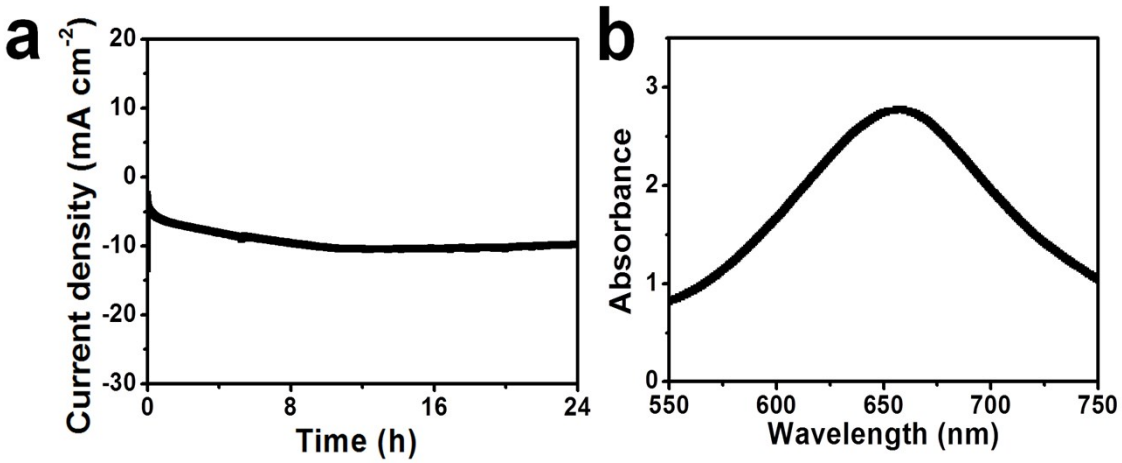

Fig. S27. Fe_2O_3-IL as catalyst in 0.1 M Na_2SO_4 electrolyte: the current density at -0.8 V *vs*. RHE for 24 h (a) and corresponding absorbance (b).

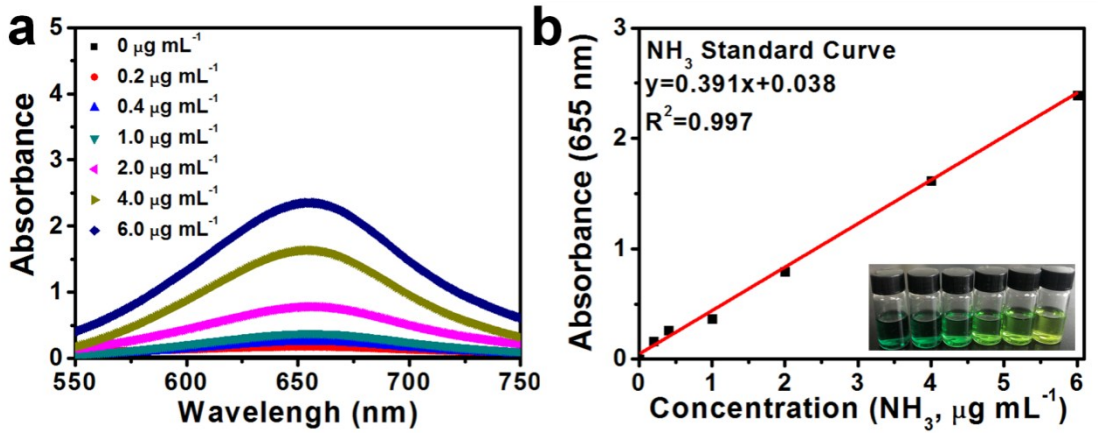

Fig. S28. In 0.001 M HCl electrolyte, the concentration-absorbance curve of NH_4^+ with concentration of 0.0, 0.2, 0.4, 1.0, 2.0, 4.0 and 6.0 μg mL^{-1} (a); calibration curve used for calculation of NH_3 by NH_4^+ concentration (b).

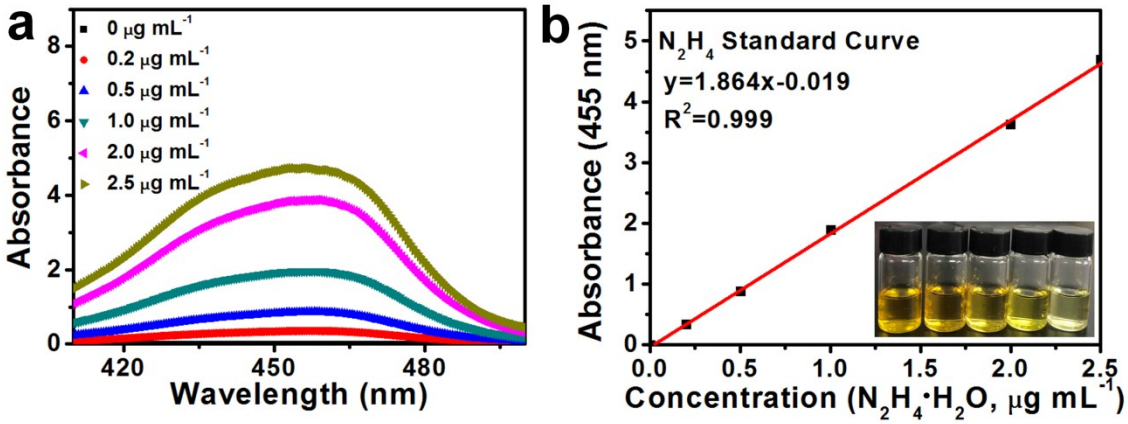

Fig. S29. In 0.001 M HCl electrolyte, the concentration-absorbance curve of N_2H_4 with concentration of 0.0, 0.2, 0.5, 1.0, 2.0 and 2.5 μg mL^{-1} (a); calibration curve used for calculation of N_2H_4 concentration (b).

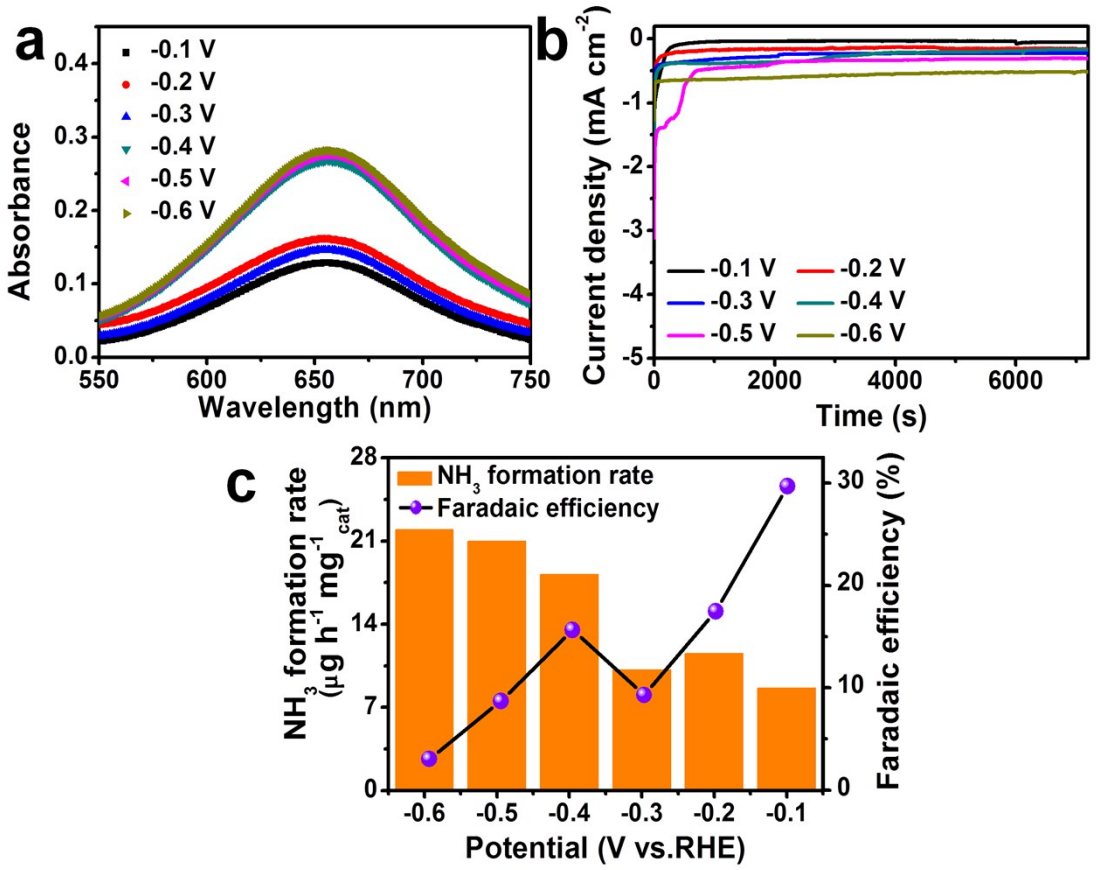

Fig. S30. Fe_2O_3-IL as catalyst in 0.001 M HCl electrolyte under the potentials from -0.1 V to -0.6 V for 2 h: UV-Vis absorption spectra of NH_3 in the electrolytes (a); the chronoamperometric test of Fe_2O_3-IL (b); NH_3 formation rates and FEs (c).

Table S4. NH_3 formation rates and the corresponding FEs of Fe_2O_3-IL under various potentials in 0.001 M HCl electrolyte.

Potential (V)	NH_3 formation rate ($\mu g\ h^{-1}\ mg^{-1}_{cat}$)	NH_3 formation rate ($mol\ s^{-1}\ cm^{-2}$)	FE (%)
-0.1	8.61	7.03×10^{-11}	29.68
-0.2	11.54	9.43×10^{-11}	17.46
-0.3	10.13	8.28×10^{-11}	9.29
-0.4	18.17	1.48×10^{-10}	15.65
-0.5	21.00	1.72×10^{-10}	8.70

-0.6	21.95	1.79×10^{-10}	3.04

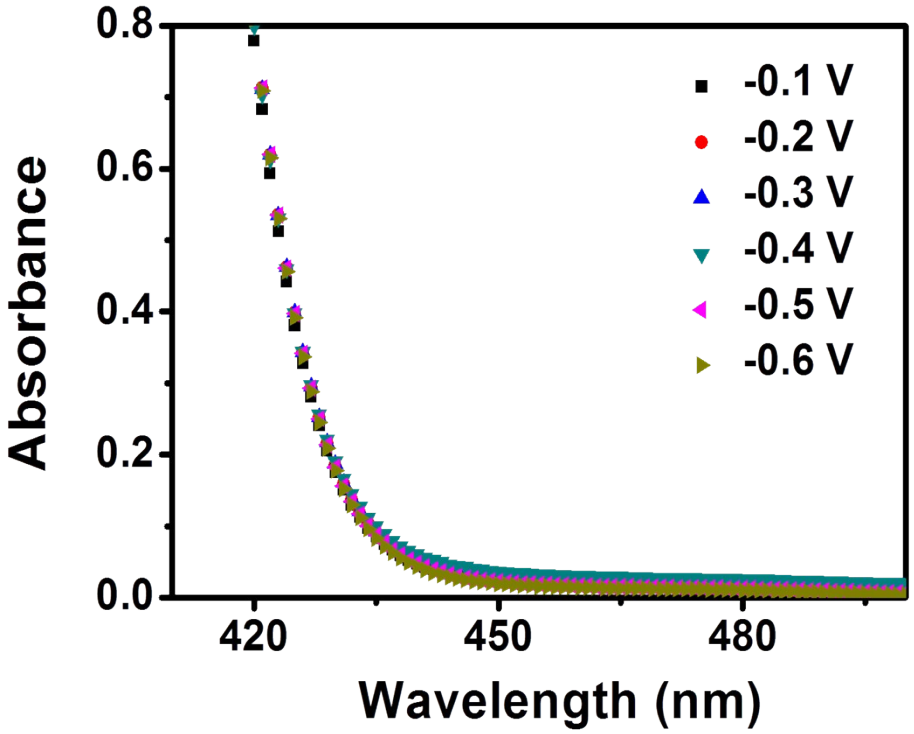

Fig. S31. The absorbance of hydrazine of Fe_2O_3-IL in 0.001 M HCl electrolyte under different potentials.

References

1 F. Zhou, L. M. Azofra, M. Ali, M. Kar, A. N. Simonov, C. J. McDonnell-Worth, C. Sun, X. Zhang and D. MacFarlane, *Energy Environ. Sci.*, 2017, **10**, 2516-2520.

2 M. Shi, D. Bao, S. Li and B. Wulan, *Adv. Energy Mater.*, 2018, **8**, 1800124.

3 J. Kong, A. Lim, C. Yoon, J. Jang, H. Ham, J. Han, S. Nam, D. Kim, Y. Sung, J. Choi and H. S. Park, *ACS Sustainable Chem. Eng.*, 2017, **5**, 10986-10995.

4 X. Xiang, Z. Wang, X. Shi, M. Fan and X. Sun, *ChemCatChem*, 2018, **10**, 4530-4535.

5 Q. Liu, X. Zhang, Z. Bing, Y. Luo, G. Cui, F. Xie and X. Sun, *Nanoscale*, 2018, **10**, 14386-14389.

6 L. Hu, A. Khaniya, J. Wang, G. Chen, W. E. Kaden and X. Feng, *ACS Catal.*, 2018, **8**, 9312-9319.

7 D. Bao, Q. Zhang, F. Meng, H. Zhong, M. Shi, Y. Zhang, J. Yan, Q. Jiang and X. Zhang, *Adv. Mater.*, 2017, **29**, 1604799.

8 H. Liu, S. Han, Y. Zhao, Y. Zhu, X. Tian, J. Zeng, J. Jiang, B. Xia, and Y. Chen, *J. Mater. Chem. A*, 2018, **6**, 3211-3217.

9 L. Zhang, X. Ji, X. Ren, Y. Ma, X. Shi, Z. Tian, A. M. Asiri, L. Chen, B. Tang and X. Sun, *Adv. Mater.*, 2018, **30**, 1800191.

10 Y. Luo, G. Chen, L. Ding, X. Chen, L. Ding and H. Wang, *Joule*, 2019, **3**, 1-11.

11 R. Zhang, X. Ren, X. Shi, F. Xie, B. Zheng, X. Guo and X. Sun, *ACS Appl. Mater. Interfaces*, 2018, **10**, 28251-28255.

12 R. Zhang, Y. Zhang, X. Ren, Y. Luo and X. P. Sun, *ACS Sustainable Chem. Eng.*, 2018, **6**, 9545-9549.

13 L. Huang, J. Wu, P. Han, A. M. Al-Enizi, T. M. Almutairi, L. Zhang and G. Zheng, *Small Methods*, 2018, **2**, 1800386.

14 M. T. Nguyen, N. Seriani and R. Gebauer, *Phys. Chem. Chem. Phys*., 2014, **17**, 14317-14322.